Observation of phase synchronization and alignment during free induction decay of quantum spins with Heisenberg interactions

Patrick Vorndamme,[1] Heinz-Jürgen Schmidt,[2] Christian Schröder,[1, 3] and Jürgen Schnack[1, *]

[1]*Faculty of Physics, Bielefeld University, 33615 Bielefeld, Germany*
[2]*Department of Physics, Osnabrück University, Barbarastraße 7, 49076 Osnabrück, Germany*
[3]*Bielefeld Institute for Applied Materials Research,*
Bielefeld University of Applied Sciences, 33619 Bielefeld, Germany
(Dated: April 14, 2021)

Equilibration of observables in closed quantum systems that are described by a unitary time evolution is a meanwhile well-established phenomenon apart from a few equally well-established exceptions. Here we report the surprising theoretical observation that non-integrable spin rings with nearest neighbor isotropic Heisenberg interaction not only equilibrate but moreover also synchronize the directions of the expectation values of the individual spins. In our numerical simulations, we investigate the free induction decay (FID) of an ensemble of up to $N = 25$ quantum spins with $s = 1/2$ each by solving the time-dependent Schrödinger equation numerically exactly. Our findings are related to, but not fully explained by conservation laws of the system. The synchronization is very robust against for instance random fluctuations of the Heisenberg couplings and inhomogeneous magnetic fields. Synchronization is not observed with strong enough anisotropic symmetry-breaking interactions such as the dipolar interaction. We also compare our results to classical spin dynamics which under all investigated conditions does not exhibit phase synchronization due to the lack of entanglement. For classical spin systems the fixed magnitude of individual spins effectively acts like additional N conservation laws.

I. INTRODUCTION

Decoherence, equilibration as well as thermalization in closed quantum systems under unitary time evolution are well-studied and by now well-established concepts which root in seminal papers by Deutsch, Srednicki and many others [1–12]. For numerical studies, spin systems are the models of choice both since they are numerically feasible due to the finite size of their Hilbert spaces as well as they are experimentally accessible for instance in standard investigations by means of electron parametric resonance (EPR), free induction decay (FID), or in atomic traps, see e.g. [13–17]. In such systems, observables assume expectation values that are practically indistinguishable from the prediction of the diagonal ensemble for the vast majority of all times of their time evolution [6, 18].

In this paper we discuss an observation that rests both on decoherence and equilibration. We study the free induction decay (FID) of quantum spins that are arranged on a ring-like geometry with nearest-neighbor isotropic Heisenberg interactions. The initial product state of single-spin states entangles, i.e. turns into a superposition of product states, and thereby equilibrates at the level of single-spin observables. Our most striking observation is that expectation values of all individual spin vectors synchronize with respect to their orientation. In a FID setting this means that their various individual rotations about the common field axis synchronize and align in the course of time. In a co-rotating frame they simply align. Experimentally, such collective effects may

e.g. be imprinted in the temporal line shapes of the optical response under ultrashort pulse excitation and thus eventually be observed [19].

The synchronization is stable against random fluctuations of the Heisenberg couplings and we observe it for almost all initial conditions. We therefore conjecture that it is tightly connected to the symmetries and conserved quantities of the isotropic Heisenberg model which is SU(2) invariant [20], see also [21]. This hypothesis is corroborated by the observation that strongly anisotropic interactions such as the dipolar interaction spoil the synchronization. Also in classical spin dynamics the phenomenon cannot be observed as will be discussed in detail later. Inhomogeneous or randomly fluctuating local fields at the sites of the individual spins on the other hand do not prevent the spins from synchronizing although the conservation laws are broken. The same applies for weakly anisotropic interactions that are close to the isotropic Heisenberg case. We observe a transient synchronization.

The paper is organized as follows. In Sect. II we introduce the theoretical model and the applied methods. Section III deals with exemplary numerical quantum simulations under isotropic Heisenberg interactions and we compare to classical simulations. Section IV introduces symmetry breaking anisotropic interactions and demonstrates the transient behaviour of the synchronization phenomenon. Section V provides a summary of our main results. In the appendix some aspects are discussed in more detail, especially the behavior under symmetry breaking interactions. Video clips of our simulations are provided on the website of the paper [22].

---

* jschnack@uni-bielefeld.de

II. THEORETICAL MODEL AND METHODS

The Hamiltonian of our spin model reads

$$\underset{\sim}{H} = -\sum_{j=1}^{N} J_j \underset{\sim}{\vec{s}}_j \cdot \underset{\sim}{\vec{s}}_{j+1} - \sum_{j=1}^{N} h_j \underset{\sim}{s}_j^z \ , \qquad (1)$$

where the first sum corresponds to the isotropic Heisenberg model and the second sum denotes the Zeeman term. Operators are marked by a tilde, the Heisenberg interactions are denoted by J_j, local magnetic fields are given by h_j, and periodic boundary conditions $s_{N+1} = s_1$ are applied. Thus, the Hamiltonian describes spins which are arranged as a ring; it could for instance be a ring molecule [23, 24]. We define the total spin operator

$$\underset{\sim}{\vec{S}} := \sum_{k=1}^{N} \underset{\sim}{\vec{s}}_k \ , \qquad (2)$$

which commutes with the Heisenberg part of the Hamiltonian, and so does $\underset{\sim}{\vec{S}}^2$, even if the coupling constants J_j are all different. This is true for any spin arrangement, not just for rings [20, 25]. The conservation of $\underset{\sim}{\vec{S}}^2$ is broken either by anisotropic interactions or by varying local magnetic fields h_j

$$\left[\underset{\sim}{\vec{S}}^2, \sum_{i=1}^{N} h_i \underset{\sim}{s}_i^z \right] \propto \underbrace{\left[\underset{\sim}{\vec{s}}_i \cdot \underset{\sim}{\vec{s}}_j, \ h_i \underset{\sim}{s}_i^z + h_j \underset{\sim}{s}_j^z \right]}_{=\ 0 \ \text{only if } h_i = h_j} \ . \qquad (3)$$

Furthermore, we define the transverse magnetization

$$\begin{aligned} M_{\text{trans}} :&= \sqrt{\langle \underset{\sim}{S}^x \rangle^2 + \langle \underset{\sim}{S}^y \rangle^2} \\ &= \sqrt{\left(\sum_j \langle \underset{\sim}{s}_j^x \rangle \right)^2 + \left(\sum_j \langle \underset{\sim}{s}_j^y \rangle \right)^2} \ . \end{aligned} \qquad (4)$$

Here $\langle \underset{\sim}{S}^x \rangle$ denotes the expectation value with respect to a specified many-body state. We interpret (4) as the net magnetization precessing in the xy-plane. In case of Hamiltonian (1) this is also a conserved quantity if the local magnetic fields are all the same $h_j \equiv h \ \forall j$. This can be seen by looking at the time evolution ($\hbar := 1$)

$$\begin{aligned} \frac{d}{dt} \langle \psi(t) | \underset{\sim}{\vec{S}} | \psi(t) \rangle &= \frac{1}{i} \langle \psi(t) | [\underset{\sim}{\vec{S}}, \underset{\sim}{H}] | \psi(t) \rangle \\ &= ih \langle \psi(t) | [\underset{\sim}{\vec{S}}, \underset{\sim}{S}^z] | \psi(t) \rangle \ . \end{aligned} \qquad (5)$$

Remember, h denotes the magnetic field. The solution of Eq. (5) is of the form

$$\langle \psi(t) | \underset{\sim}{\vec{S}} | \psi(t) \rangle = \begin{pmatrix} a \cos ht + b \sin ht \\ -b \cos ht + a \sin ht \\ c \end{pmatrix} \ , \qquad (6)$$

compatible with the conserved quantities. The coefficients a, b and c are determined by the initial state of the system. We observe a collective rotation with frequency h in all cases the spins synchronize (Sections III A, III B and III D). Appendix B 1 provides an exception where the spins collectively precess around a mean field $\tilde{h}$.

As initial many-body states we choose product states of the form

$$|\psi(t=0)\rangle = \bigotimes_{j=1}^{N} \frac{1}{\sqrt{2}} \left(|\uparrow\rangle + e^{i\theta_j} |\downarrow\rangle \right) \ , \qquad (7)$$

for which the expectation values of individual spins

$$\langle \underset{\sim}{\vec{s}}_j \rangle := \langle \psi | \underset{\sim}{\vec{s}}_j | \psi \rangle \qquad (8)$$

are oriented in the xy-plane and point in a direction that depends on θ_j. In the following we are going to investigate the time evolution of the four states shown in Fig. 1 where (a) all spins point in the same direction, (b) are regularly fanned out by 180 degrees, (c) are regularly fanned out by 360 degrees, and (d) point in random directions. We will refer to this states as $|\psi_A\rangle$, $|\psi_B\rangle$, $|\psi_C\rangle$, and $|\psi_D\rangle$ (or A, B, C, and D in the classical case, sec. III E).

(a) 0 degrees   (b) 180 degrees
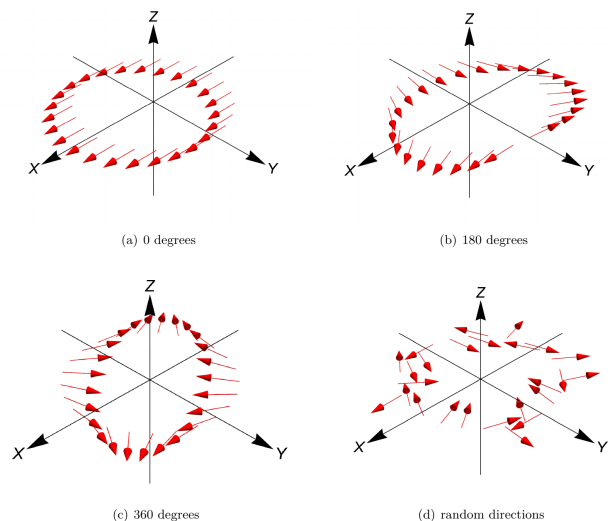
(c) 360 degrees   (d) random directions

FIG. 1. Visualization of the four initial product states studied in this work. The arrows correspond to the single-spin expectation values, see text and Eq. (7). We will refer to this states as $|\psi_A\rangle$, $|\psi_B\rangle$, $|\psi_C\rangle$, and $|\psi_D\rangle$.

In a product state, the spins are not entangled by definition, however they entangle during the unitary time evolution

$$|\psi(t)\rangle = e^{-i\underset{\sim}{H}t} |\psi(0)\rangle \ , \qquad (9)$$

that we calculate numerically exactly using a Suzuki Trotter decomposition [26].

In order to measure the entanglement of an individual spin at site j with the others, we define the reduced density matrix

$$\underset{\sim}{\rho}_j = \text{Tr}_{\bigotimes_{k \neq j} \mathscr{H}_k} (|\psi\rangle \langle \psi|) \ . \qquad (10)$$

Here $\mathcal{H}_j$ denotes the Hilbert subspace of spin j, and $\mathcal{H} = \bigotimes\limits_{j=1}^{N} \mathcal{H}_j$ is the total Hilbert space. The purity is given as $Tr\left(\underset{\sim}{\rho}_j^2\right)$. $Tr\left(\underset{\sim}{\rho}_j^2\right) = 1$ holds, if spin j is not entangled with other spins, and $Tr\left(\underset{\sim}{\rho}_j^2\right) = 0.5$ if it is maximally entangled with other spins. The purity is thus also a measure of decoherence for an observer of a single spin [27, 28]. An alternative way of quantifying the decoherence would be the von Neumann entropy $S(\underset{\sim}{\rho}_j) = -Tr\left(\underset{\sim}{\rho}_j \log_2 \underset{\sim}{\rho}_j\right)$ [29].

III.   CALCULATIONS AND RESULTS

In this Section we present our numerical findings of the special behaviour of initial states in Fig. 1 under time evolution with Hamiltonian Eq. (1) and equal magnetic fields $h_j = -1 \; \forall j$. As discussed, M_{trans} and $\underset{\sim}{\vec{S}^2}$ are conserved quantities. We show that, with one exception, the spin expectation values synchronize.

A.   Initial state $|\psi_A\rangle$

In Fig. 2 we start with initial state $|\psi_A\rangle$ and random Heisenberg interactions J_j. In this case, every spin is precessing as if independent without entangling to other spins, no matter how the J_j are chosen. Since all spins point in the same direction, M_{trans} and $\underset{\sim}{\vec{S}^2}$ assume their maximum values. Because they are conserved quantities the spins are bound to remain in a perfect product state, otherwise it would not be possible to conserve these values over time.
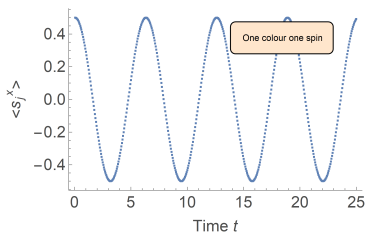

FIG. 2.   Time evolution of initial state $|\psi_A\rangle$ regarding Hamiltonian Eq. (1) with isotropic Heisenberg interactions and $J_j \in [1.6, 2.4]$, $h_j = -1 \; \forall j$, $N = 25$.

B.   Initial state $|\psi_B\rangle$

Figure 3 shows almost the same as Fig. 2, but this time for initial state $|\psi_B\rangle$. Initially the individual spin expectation values are spread out by 180 degrees, but during time evolution they align. This astonishing phenomenon

can be nicely observed in the video provided on the web page of the published article [22].

During time evolution and synchronization the spins entangle as much as the conservation of $\underset{\sim}{\vec{S}^2}$ and M_{trans} allows. Interestingly, the spins stay entangled and do not fan out again (apart from finite size effects such as revivals at very late times). This statement becomes stronger with increasing system size, which is further addressed in Appendix A. We interpret this phenomenon as quantum mechanical equilibration process under the restricting influence of conserved quantities [21].

The synchronization can be rationalized for spin systems where all spins are equivalent, i.e. ring systems with translational invariance ($J_j = J$, $h_j = h \; \forall j$) since then equilibration should result in the same single-spin expectation value at every site. This concerns magnitude and direction of the spin vector. The somewhat unexpected result of our investigation is that the direction of all spins continues to synchronize also for settings where spins are no longer equivalent, i.e. if the Heisenberg interactions are drawn at random from a distribution.
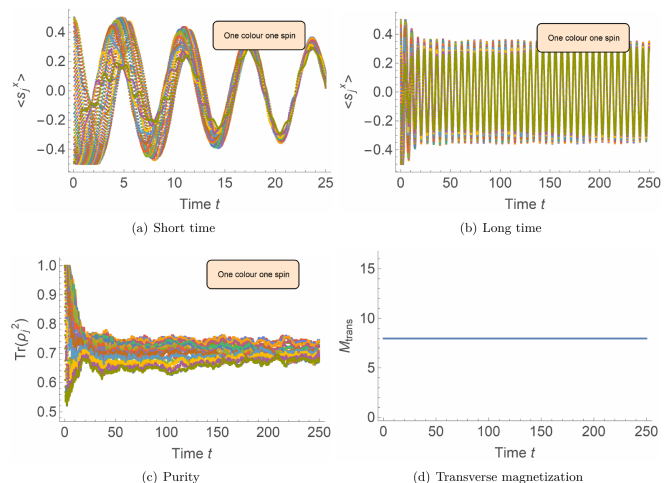

FIG. 3.   Time evolution of initial state $|\psi_B\rangle$ w.r.t. Hamiltonian Eq. (1) with isotropic Heisenberg interactions and $J_j \in [1.6, 2.4]$, $h_j = -1 \; \forall j$, $N = 25$. The video for 3(a) can be found at [22].

Figure 3(c) shows the purity of the individual reduced density operators $\underset{\sim}{\rho}_j$ (Eq. (10)). Since the couplings J_j are different for different j, not all spins are equal. This does not prevent the spins from synchronizing their directions, but they do not all entangle to the same extent.

Another main result of this paper is that the time needed for the spins to synchronize is almost independent of the width Δ of the distribution of the $J_j \in [2 - \Delta, 2 + \Delta]$. This is also demonstrated numerically in Appendix A.
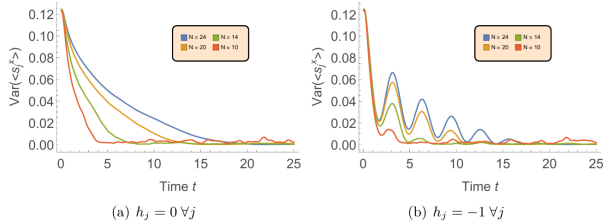
Figure 4 shows the variance of the expectation values

(a) $h_j = 0 \ \forall j$

(b) $h_j = -1 \ \forall j$

FIG. 4. Time evolution of initial state $|\psi_B\rangle$ w.r.t. Hamiltonian Eq. (1) with isotropic Heisenberg interactions and $J_j = 2 \ \forall j$ without (a) and with magnetic field (b).

of individual spin operators, defined as

$$\mathsf{Var}(< \underset{\sim}{s}_j^x >)(t) := \frac{1}{N} \sum_{j=1}^{N} \left(< \underset{\sim}{s}_j^x > - \frac{< S^x >}{N} \right)^2 \quad (11)$$

for different system sizes N. That the variance decays to zero, compare Fig. 4, expresses precisely that the spins align until they point in the same direction. This process takes the longer the larger the system is. The synchronisation, i.e. the alignment of directions, also takes place in the absence of a magnetic field, as can be seen in Fig. 4(a). The reason is that the homogeneous magnetic field, which is a one-body operator, does not causes any many-body entanglement between the spins; entanglement and equilibration are driven by the Heisenberg term which is a two-body operator. As a result, the field-free curves in Fig. 4(a) are the envelopes of the curves taken at homogeneous field and shown in Fig. 4(b).

C. Initial state $|\psi_C\rangle$

Figure 5 shows the time evolution for initial state $|\psi_C\rangle$ and different system sizes. This is a very special and atypical case with a particular symmetry in the spin orientations which results in a very stable state even if there are different couplings J_j between the spins, see video [22]. This is the only initial state we find where the spins do not align, but entangle and decay to zero, with wild echos at later times. The larger the system, the longer the echos take to occur and the longer it takes for the spins to entangle.

These numerical results for finite system sizes suggest that $|\psi_C\rangle$ is an energy eigenstate in the thermodynamic limit which appears plausible, because the angle between neighboring spins is given by $2\pi/N$, therefore for $N \to \infty$ all neighbors are parallel in the initial state. We emphasize that this state would also be an energy eigenstate in the non-integrable case [30, 31] where the J_j are all different. Because all single-spin observables are strongly different we conjecture that this state is not thermal; its relation to quantum scars needs to be explored, see [32, 33] and references therein.

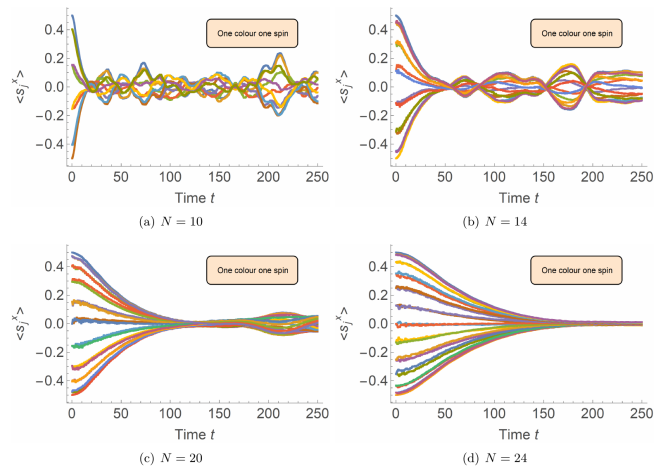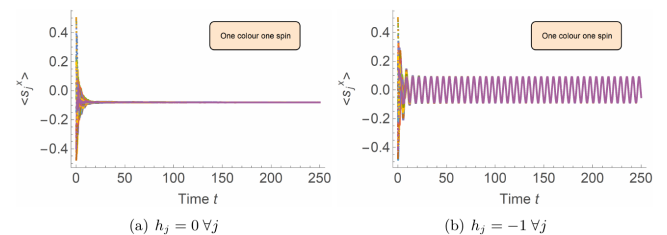(a) $N = 10$

(b) $N = 14$

(c) $N = 20$

(d) $N = 24$

FIG. 5. Time evolution of initial state $|\psi_C\rangle$ w.r.t. Hamiltonian Eq. (1) with isotropic Heisenberg interactions and $J_j \in [1.6, 2.4]$, $h_j = 0 \ \forall j$ and for various system sizes. The videos of 5(d) is provided at [22].

D. Initial state $|\psi_D\rangle$

(a) $h_j = 0 \ \forall j$

(b) $h_j = -1 \ \forall j$

FIG. 6. Time evolution of initial state $|\psi_D\rangle$ w.r.t. Hamiltonian Eq. (1) with isotropic Heisenberg interactions and $J_j \in [1.6, 2.4]$, $N = 24$ without (a) and with magnetic field (b). Video 6(b) is provided at [22].

Figure 6 shows a time evolution for initial state $|\psi_D\rangle$ (random orientations) without magnetic field (Fig. 6(a)) and with magnetic field (Fig. 6(b)). The conserved net magnetization is small (would be zero in the thermodynamic limit or as a mean of many random realizations according to the central limit theorem). Nevertheless, the spins synchronize which shows that this phenomenon is very robust with respect to the initial state, see also video [22].

E. Classical spin dynamics

We now compare our results to classical spin dynamics. It runs out that a classical spin dynamics does not exhibit phase synchronization, see videos [22]. The reason in this context is that classical spin dynamics lacks entanglement. Contrary to the expectation values of the

quantum spins, the classical spins are bound to maintain their length, which effectively acts like additional N conservation laws. This results in a oscillatory dynamics of all investigated initial conditions, compare Fig. 7 for initial states equivalent to Fig. 2(b)-(d).

The classical spin dynamics has been evaluated according to

$$\frac{d}{dt}\vec{s}_j = \frac{\partial H}{\partial \vec{s}_j} \times \vec{s}_j \ , \tag{12}$$

where H denotes the classical Hamiltonian analogous to Eq. (1).

(a) Initial state B, $h = 0 \ \forall j$

(b) Initial state B, $h = -1 \ \forall j$

(c) Initial state C, $h = 0 \ \forall j$

(d) Initial state D, $h = 0 \ \forall j$
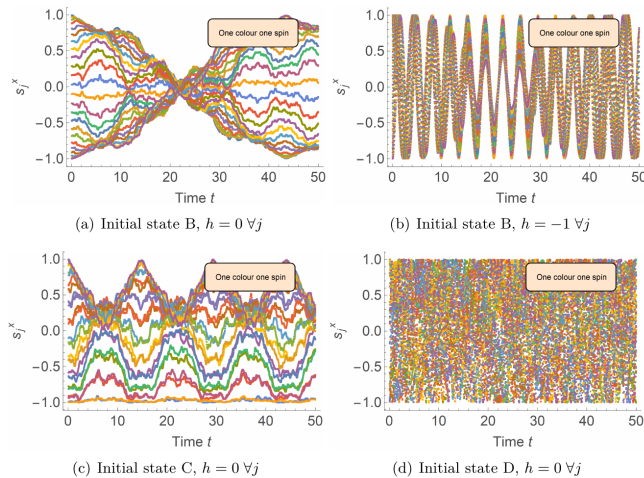
FIG. 7. Classical time evolution with $N = 24$, $J_j \in [1.6, 2.4]$. Videos for all cases are provided at [22].

Interestingly the classical spins for initial state B seem to try to synchronize their directions (Fig. 7(a)-(b)). At one point in time their projections to the xy-plane point in the same direction. But as time goes on, they loose their temporal alignment.

IV. BREAKING THE SYMMETRY

In this Section we investigate whether synchronization still occurs if M_{trans} and $\vec{\underset{\sim}{S}}^2$ are not conserved anymore. We can break the symmetry in different ways, either by means of inhomogeneous magnetic fields or by interactions between the spins that are not of isotropic Heisenberg type. In Section (IV A) we choose XYZ interactions and in Section (IV B) XX interactions as two examples with different outcomes. In Appendix B we show the effect of inhomogeneous magnetic fields (App. B 1) and of dipolar interactions between all spins (App. B 2).

A. XYZ interaction

We begin with the XYZ interaction which is close to the isotropic Heisenberg case if the interaction in the three spatial directions is not too different. In this case, the synchronization between the spins still occurs. The Hamiltonian in this subsection is defined as

$$\underset{\sim}{H}_{XYZ} = - J \sum_{j=1}^{N} \underset{\sim}{s}_j^x \underset{\sim}{s}_{j+1}^x - (J - \delta) \sum_{j=1}^{N} \underset{\sim}{s}_j^y \underset{\sim}{s}_{j+1}^y$$
$$- (J - 2\delta) \sum_{j=1}^{N} \underset{\sim}{s}_j^z \underset{\sim}{s}_{j+1}^z - h \sum_{j=1}^{N} \underset{\sim}{s}_j^z \ . \tag{13}$$

We use the parameter δ to tune the difference of the interaction in the three spatial directions.

(a) $< s_j^x >$, $\delta = 0.05$

(b) $Tr\left(\rho_j^2\right)$, $\delta = 0.05$

(c) $< s_j^x >$, $\delta = 0.2$

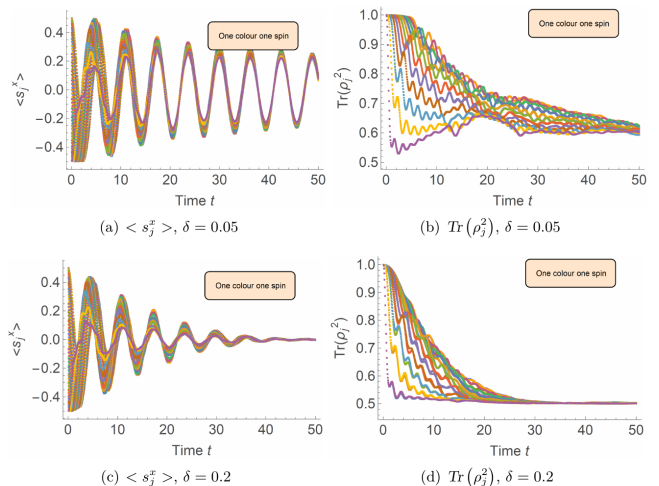(d) $Tr\left(\rho_j^2\right)$, $\delta = 0.2$

FIG. 8. Time evolutions of initial state $|\psi_B\rangle$ w.r.t. Hamiltonian Eq. (13) for two values of δ, and $N = 24$, $J = 2$, $h = -1$. Videos of 8(a) and (c) are provided at [22].

Figure 8 shows time evolutions for initial state $|\psi_B\rangle$ and two different values of δ. The magnetization is not a conserved quantity anymore and will therefore decay towards its equilibrium value, which is zero in the xy-plane for a magnetic field in z-direction. Our investigations reveal that the larger δ the faster the spins decay. However, we clearly observe that while decaying the spins still synchronize, see especially Fig. 8(a). One could say, that the synchronization is a transient phenomenon in such cases since the time scale of synchronization is shorter than that of the unavoidable decay.

Fugure 8(b) and Fig. 8(d) show the purity of the reduced density operators $\underset{\sim}{\rho}_j$ introduced in Eq. (10).We see that all spins maximally entangle ($Tr\left(\underset{\sim}{\rho}_j^2\right) = 0.5$) which is equivalent with all individual spin expectation values decay to zero.

Another example of broken symmetry where the spins still synchronize is shown in Appendix B 1 with an inhomogeneous magnetic field.

B.   XX interaction

As comparison we now show a case with XX interaction where the spins do not synchronize. The Hamiltonian is defined as

$$\underset{\sim}{H}_{XX} = -J \sum_{j=1}^{N} \left(\underset{\sim}{s}_j^x \underset{\sim}{s}_{j+1}^x + \underset{\sim}{s}_j^y \underset{\sim}{s}_{j+1}^y \right) - h \sum_{j=1}^{N} \underset{\sim}{s}_j^z \ . \quad (14)$$

Figure 9 shows a time evolution for initial state $|\psi_B\rangle$. The decay of the transverse magnetization is much faster than in the previous subsection, because we are further away from isotropic Heisenberg interactions and the symmetry regarding the conservation of the transverse magnetization is broken much more strongly, compare also [17]. In order to see if the spins still synchronize while decaying to zero, we choose a much smaller coupling constant $J = 0.1$ instead $J = 2$. But we clearly see that the spins do not synchronize while decaying or equivalently the timescale of the decay is much higher than the timescale of synchronization.
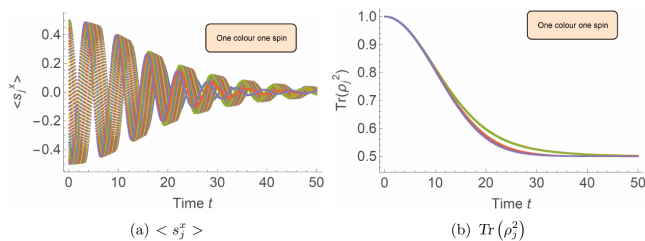

FIG. 9.   Time evolution of initial state $|\psi_B\rangle$ w.r.t. Hamiltonian Eq. (14) with parameters $N = 24$, $J = 0.1$ and $h = -1$. The video of 9(a) can be found at [22].

Another example of broken symmetry where the spins do not synchronize is shown in Appendix B 2 with dipolar interactions between the spins.

V.   SUMMARY

As a conclusion we can say first of all that conservation of M_{trans} and $\vec{\underset{\sim}{S}}^2$ not just slows down the FID, but prevents the free induction from decaying if the Hamiltonian only contains isotropic Heisenberg interactions and

all Zeeman terms of the spins are equal (see Fig. 2). This is in accord with Ref. [21].

Furthermore we demonstrate in detail the interesting phenomenon that the single spin vector expectation values align in the course of time almost independent of how they are initialized in the xy-plane (see Fig. 3). For this process, the magnetic field is not necessary, it only induces a (collective) rotation of all spins about the field axis (see e.g. Fig. 4 and Fig. 10). The Heisenberg interactions cause an equilibration process under the constraint of conserved quantities. We show that after entanglement is maximised (under constraints of conserved quantities) and equilibration is completed the spins stay synchronized and fluctuate less the larger the system is (see e.g. Fig. 13, Apppendix A). Moreover, we show that the timescale of synchronization is independent of the width Δ of the variation of Heisenberg couplings J_j (see Fig. 14, Apppendix A).

We demonstrate that such a synchronization is not possible with classical spins (see Fig. 7).

In addition, we discuss that the synchronization of spin expectation values is very robust. It happens already for small systems ($N = 10$, see Fig. 12, Apppendix A) and for various initial states (see e.g. Fig. 6). We find just one exception (initial state $|\psi_C\rangle$) which in the thermodynamic limit becomes an energy eigenstate (see Fig. 5).

Further on, we provide examples of transient synchronization for systems where symmetries are broken, because the time scale of synchronization is shorter than that of equilibration. Systems with anisotropic XYZ interactions belong to this set if they are still close to the isotropic Heisenberg case (see Fig. 8), or if the symmetry is broken by means of an inhomogeneous magnetic field (see Fig. 15 and Apppendix B 1, respectively).

Finally we show that the spins do not synchronize for interactions that are strongly anisotropic such as dipolar interactions (see Fig. 17, Appendix B 2).

Our investigations might be helpful for interpreting observations in the context of FID.

ACKNOWLEDGMENT

[1] J. M. Deutsch, Quantum statistical mechanics in a closed system, Phys. Rev. A **43**, 2046 (1991).

[2] M. Srednicki, Chaos and quantum thermalization, Phys. Rev. E **50**, 888 (1994).

[3] J. Schnack and H. Feldmeier, Statistical properties of fermionic molecular dynamics, Nucl. Phys. A **601**, 181 (1996).

[4] M. Rigol, V. Dunjko, and M. Olshanii, Thermalization and its mechanism for generic isolated quantum systems,

Nature **452**, 854 (2008).

[5] A. Polkovnikov, K. Sengupta, A. Silva, and M. Vengalattore, Colloquium, Rev. Mod. Phys. **83**, 863 (2011).

[6] P. Reimann and M. Kastner, Equilibration of isolated macroscopic quantum systems, New Journal of Physics **14**, 043020 (2012).

[7] R. Steinigeweg, A. Khodja, H. Niemeyer, C. Gogolin, and J. Gemmer, Pushing the limits of the eigenstate thermalization hypothesis towards mesoscopic quantum systems, Phys. Rev. Lett. **112**, 130403 (2014).

[8] C. Gogolin and J. Eisert, Equilibration, thermalisation, and the emergence of statistical mechanics in closed quantum systems, Rep. Prog. Phys. **79**, 056001 (2016).

[9] L. D'Alessio, Y. Kafri, A. Polkovnikov, and M. Rigol, From quantum chaos and eigenstate thermalization to statistical mechanics and thermodynamics, Adv. Phys. **65**, 239 (2016).

[10] F. Borgonovi, F. M. Izrailev, L. F. Santos, and V. G. Zelevinsky, Quantum chaos and thermalization in isolated systems of interacting particles, Phys. Rep. **626**, 1 (2016).

[11] Y.-L. Wu, D.-L. Deng, X. Li, and S. Das Sarma, Intrinsic decoherence in isolated quantum systems, Phys. Rev. B **95**, 014202 (2017).

[12] P. Vorndamme and J. Schnack, Decoherence of a singlet-triplet superposition state under dipolar interactions of an uncorrelated environment, Phys. Rev. B **101**, 075101 (2020).

[13] S. A. Crooker, D. D. Awschalom, J. J. Baumberg, F. Flack, and N. Samarth, Optical spin resonance and transverse spin relaxation in magnetic semiconductor quantum wells, Phys. Rev. B **56**, 7574 (1997).

[14] N. Mizuochi, P. Neumann, F. Rempp, J. Beck, V. Jacques, P. Siyushev, K. Nakamura, D. J. Twitchen, H. Watanabe, S. Yamasaki, F. Jelezko, and J. Wrachtrup, Coherence of single spins coupled to a nuclear spin bath of varying density, Phys. Rev. B **80**, 041201 (2009).

[15] Ł. Cywiński, W. M. Witzel, and S. D. Sarma, Electron spin dephasing due to hyperfine interactions with a nuclear spin bath, Physical Review Letters **102**, 057601 (2009).

[16] A. Ardavan, O. Rival, J. J. L. Morton, S. J. Blundell, A. M. Tyryshkin, G. A. Timco, and R. E. P. Winpenny, Will spin-relaxation times in molecular magnets permit quantum information processing?, Phys. Rev. Lett. **98**, 057201 (2007).

[17] P. N. Jepsen, W. W. Ho, J. Amato-Grill, I. Dimitrova, E. Demler, and W. Ketterle, Transverse spin dynamics in the anisotropic Heisenberg model realized with ultracold atoms, (2021), arXiv:2103.07866 [cond-mat.quant-gas].

[18] B. N. Balz and P. Reimann, Typical relaxation of isolated many-body systems which do not thermalize, Phys. Rev. Lett. **118**, 190601 (2017).

[19] S. Weiss, M.-A. Mycek, J.-Y. Bigot, S. Schmitt-Rink, and D. S. Chemla, Collective effects in excitonic free induction decay: Do semiconductors and atoms emit coherent light in different ways?, Phys. Rev. Lett. **69**, 2685 (1992).

[20] R. Schnalle and J. Schnack, Calculating the energy spectra of magnetic molecules: application of real- and spin-space symmetries, Int. Rev. Phys. Chem. **29**, 403 (2010).

[21] G. S. Uhrig, J. Hackmann, D. Stanek, J. Stolze, and F. B. Anders, Conservation laws protect dynamic spin correlations from decay: Limited role of integrability in the central spin model, Phys. Rev. B **90**, 060301 (2014).

[22] Videos are provided as supplementary material and at https://obelix.physik.uni-bielefeld.de/~schnack/index-publications.html.

[23] F. Troiani, A. Ghirri, M. Affronte, S. Carretta, P. Santini, G. Amoretti, S. Piligkos, G. Timco, and R. Winpenny, Molecular engineering of antiferromagnetic rings for quantum computation, Phys. Rev. Lett. **94**, 207208 (2005).

[24] J. Ummethum, J. Nehrkorn, S. Mukherjee, N. B. Ivanov, S. Stuiber, T. Strässle, P. L. W. Tregenna-Piggott, H. Mutka, G. Christou, O. Waldmann, and J. Schnack, Discrete antiferromagnetic spin-wave excitations in the giant ferric wheel Fe_{18}, Phys. Rev. B **86**, 104403 (2012).

[25] K. Bärwinkel, H.-J. Schmidt, and J. Schnack, Structure and relevant dimension of the Heisenberg model and applications to spin rings, J. Magn. Magn. Mater. **212**, 240 (2000).

[26] N. Hatano and M. Suzuki, Finding exponential product formulas of higher orders, in *Quantum Annealing and Other Optimization Methods*, edited by A. Das and B. K. Chakrabarti (Springer Berlin Heidelberg, Berlin, Heidelberg, 2005) pp. 37–68.

[27] M. Schlosshauer, Decoherence, the measurement problem, and interpretations of quantum mechanics, Rev. Mod. Phys. **76**, 1267 (2005).

[28] M. Schlosshauer, The quantum-to-classical transition and decoherence, ArXiv e-prints (2014), arXiv:1404.2635 [quant-ph].

[29] H. C. Donker, H. D. Raedt, and M. I. Katsnelson, Decoherence and pointer states in small antiferromagnets: A benchmark test, SciPost Phys. **2**, 010 (2017).

[30] H. Babujian, Exact solution of the isotropic Heisenberg chain with arbitrary spins: Thermodynamics of the model, Nucl. Phys. B **215**, 317 (1983).

[31] H. Frahm, N.-C. Yu, and M. Fowler, The integrable xxz Heisenberg model with arbitrary spin: Construction of the hamiltonian, the ground-state configuration and conformal properties, Nucl. Phys. B **336**, 396 (1990).

[32] S. Choi, C. J. Turner, H. Pichler, W. W. Ho, A. A. Michailidis, Z. Papić, M. Serbyn, M. D. Lukin, and D. A. Abanin, Emergent su(2) dynamics and perfect quantum many-body scars, Phys. Rev. Lett. **122**, 220603 (2019).

[33] S. Pilatowsky-Cameo, D. Villaseñor, M. A. Bastarrachea-Magnani, S. Lerma-Hernández, L. F. Santos, and J. G. Hirsch, Ubiquitous quantum scarring does not prevent ergodicity, Nat. Commun. **12**, 852 (2021).

Appendix A: Additions to section III

Here we present more detailed numerical calculations regarding Section (III B).

In Fig. 10 the purity of individual reduced density matrices is shown for different system sizes N. All Heisenberg couplings J_j are chosen equal and therefore all spins entangle in an equal way during equilibration (in contrast to Fig. 3(c)). It can be clearly seen that the respective purities fluctuate less the larger the system is. Thus, in the thermodynamic limit ($N \to \infty$) we expect them to keep the same order of magnitude without fluctuating after equilibration. This figure is completely independent of the strength of the magnetic field h, because the Zee-
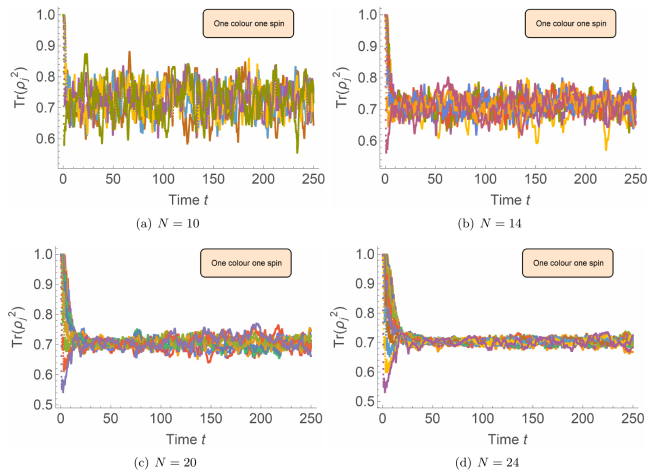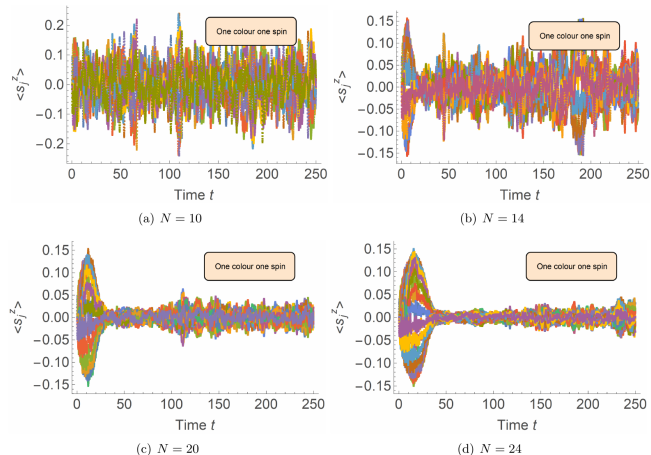
FIG. 10. Time evolution of initial state $|\psi_B\rangle$ w.r.t. Hamiltonian Eq. (1) with isotropic Heisenberg interactions and $J_j = 2 \ \forall j$, $h_j \equiv h \ \forall j$. The value of h does not change this figure.

man term in Hamiltonian Eq. (1) causes no entanglement between spins.

FIG. 11. Time evolution of initial state $|\psi_B\rangle$ w.r.t. Hamiltonian Eq. (1) with isotropic Heisenberg interactions and $J_j = 2 \ \forall j$, $h_j \equiv -1 \ \forall j$.

Figure 11 shows the individual $\langle s_j^z \rangle$ expectation values for the exact same time evolutions as Fig. 10. Initially all these values are zero because the spins are oriented in the xy-plane (see Fig. 1). During time evolution (especially at the beginning) the spins leave the xy-plane, but at later times these fluctuations in z-direction become small for a larger system size N.

Figure 12 and Fig. 13 show individual spin expectation values for time evolutions without magnetic field for different system sizes and for short and long time (also for initial state $|\psi_B\rangle$). It can be qualitatively seen that such synchronization of spins can already be observed for a small system size of $N = 10$. For $N = 6$ the spins fluc-

tuate much and for $N = 2$ the spins permanently point in opposite directions.
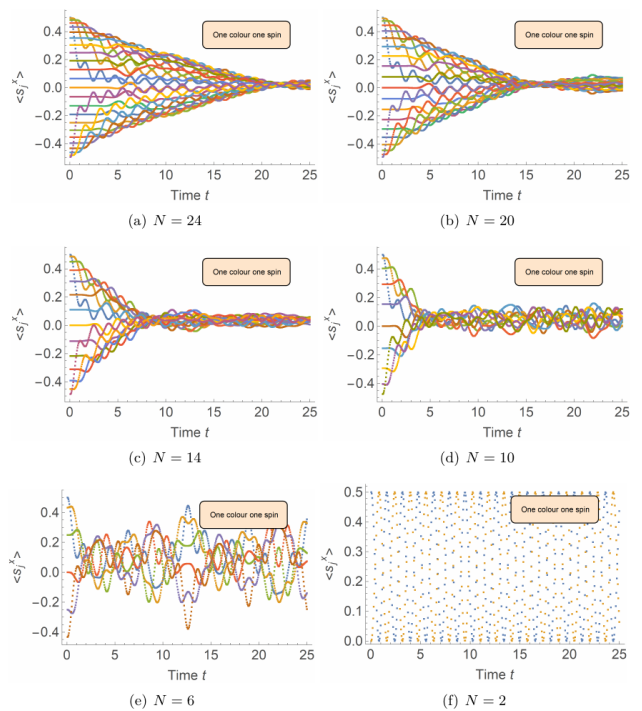

FIG. 12. Time evolution of initial state $|\psi_B\rangle$ w.r.t. Hamiltonian Eq. (1) with isotropic Heisenberg interactions and $J_j = 2 \ \forall j$, $h_j = 0 \ \forall j$ (short time).

We now want to focus on the question how the choice of couplings J_j influences the time needed for the spins to align. This is addressed by Fig. 14. The couplings J_j are chosen randomly from intervals of different width Δ and the magnetic field is zero. We see that Δ has a very small impact on the time evolution and the behaviour of the spins; the process of alignment and the time it takes is very robust. The time to synchronization does only depend on the system size N and the mean J_j.

Appendix B: Additions to section IV

In addition to sec. IV, here we present more cases of how the spins behave with broken symmetry (without the conserved quantities M_{trans} and $\underset{\sim}{\vec{S}^2}$).

1. Inhomogeneous magnetic field

As shown in Eq. (3) all magnetic fields h_j have to be equal or the conserved quantities are broken.

Figure 15 shows time evolutions of initial state $|\psi_B\rangle$ where only a few spins see a magnetic field $h_j = h \neq 0$ and all others fields are zero. Surprisingly the spins do still synchronize an precess together while they decay.
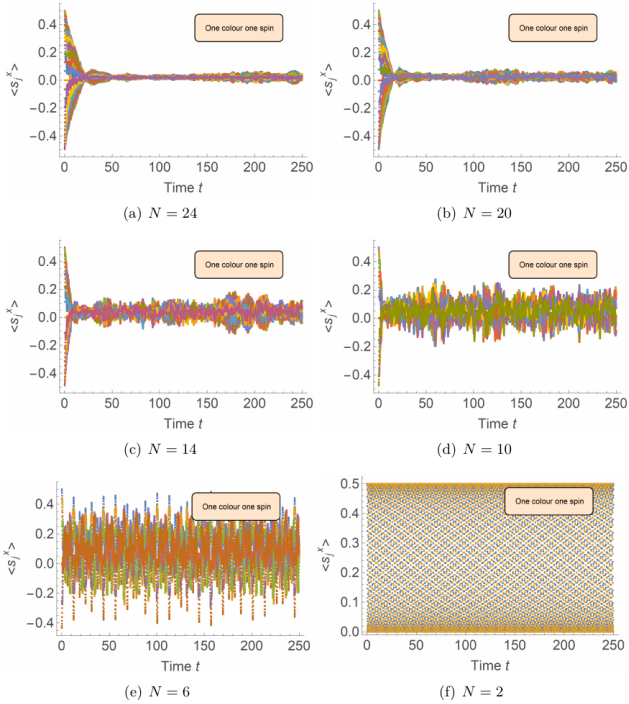
FIG. 13. Time evolution of initial state $|\psi_B\rangle$ w.r.t. Hamiltonian Eq. (1) with isotropic Heisenberg interactions and $J_j = 2\ \forall j$, $h_j = 0\ \forall j$ (long time).

The spins without magnetic field are carried with the others.

The frequency $\tilde{h}$ of the collective precession decreases the more spins there are with $h_j = 0$. This can be viewed as every spin sees a mean field $\tilde{h} = \sum_j h_j / N$. From Fig. 15(a) to Fig. 15(c) the number of magnetic fields $h_j = h$ is halved and the precession frequency $\tilde{h}$ also halves.

Another way of breaking the symmetry is by choosing random magnetic fields. Figure 16 shows time evolutions for initial state $|\psi_B\rangle$ where the magnetic fields h_j are drawn at random from a distribution of different width ξ. The spins do still synchronize up to large values of ξ up to the point where the decay of the transverse magnetization is faster than the synchronization.

2. Dipolar interactions

We now investigate how initial state $|\psi_B\rangle$ behaves when all spins (not only neighbors) interact with dipolar interactions. The Hamiltonian of such systems is given by
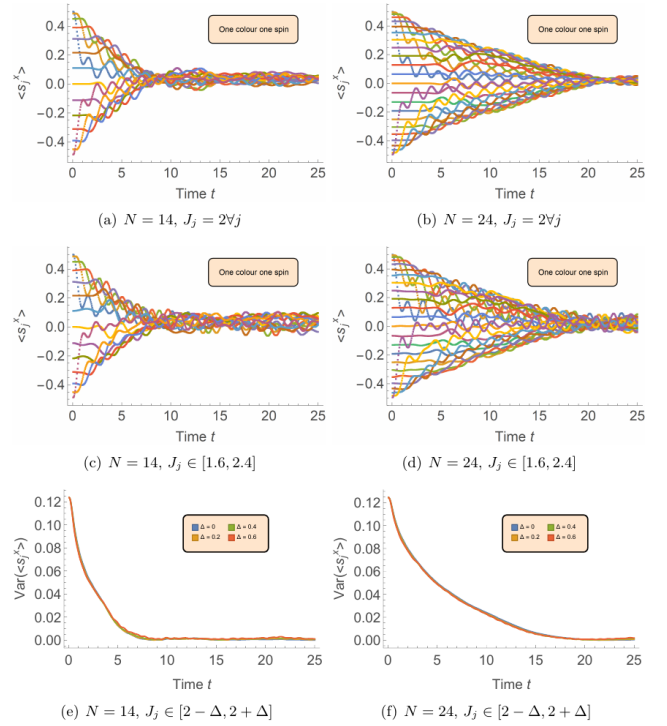

FIG. 14. Time evolution of initial state $|\psi_B\rangle$ w.r.t. Hamiltonian Eq. (1) with isotropic Heisenberg interactions from intervals of different width Δ, $J_j \in [2 - \Delta, 2 + \Delta]$ and different system sizes N, $h_j = 0\ \forall j$.
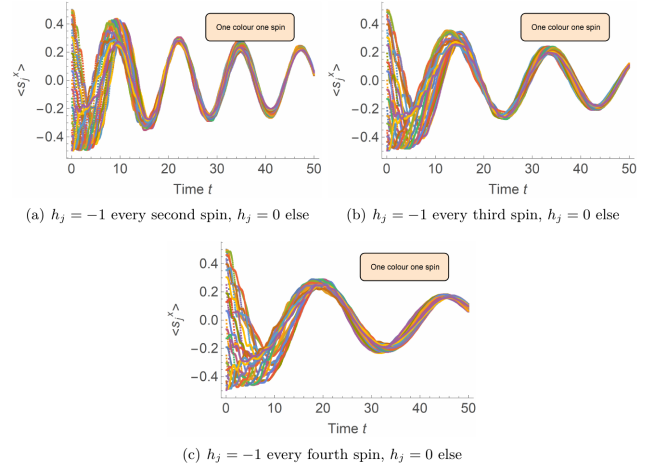

FIG. 15. Time evolution of initial state $|\psi_B\rangle$ w.r.t. Hamiltonian Eq. (1) with isotropic Heisenberg interactions and $J_j = 2\ \forall j$, $N = 24$ and for different configurations of h_j. Videos of 15(a) and (c) are provided at [22].

(a) $\xi = 0.1$

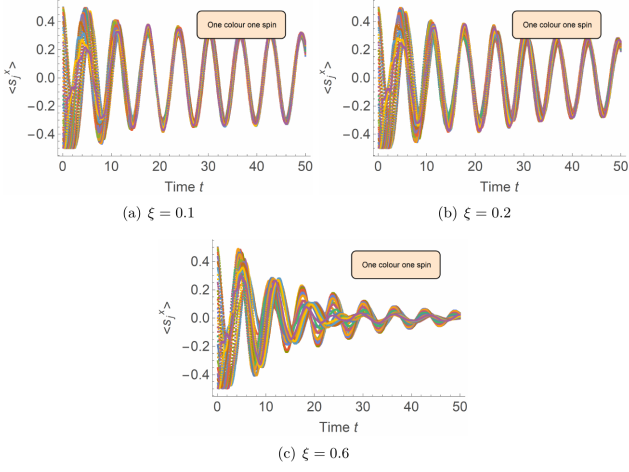(b) $\xi = 0.2$

(c) $\xi = 0.6$

FIG. 16. Time evolution of initial state $|\psi_B\rangle$ w.r.t. Hamiltonian Eq. (1) with isotropic Heisenberg interactions, $J_j = 2 \ \forall j$, $N = 24$ and $h_j \in [-1-\xi, -1+\xi]$. Videos of 16(a) and (c) are provided at [22].

(a) $< s_j^x >$, $\lambda = 0.00125$

(b) $Tr\left(\rho_j^2\right)$, $\lambda = 0.00125$

(c) $< s_j^x >$, $\lambda = 0.005$
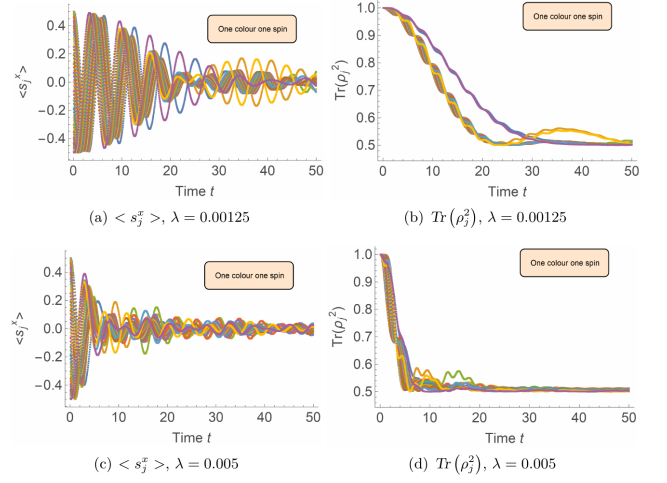
(d) $Tr\left(\rho_j^2\right)$, $\lambda = 0.005$

FIG. 17. Time evolution of initial state $|\psi_B\rangle$ w.r.t. Hamiltonian Eq. (B1) with coordinates Eq. (B2), $N = 24$ and for different parameters λ. The video of 17(a) can be found at [22].

We use the parameter λ to tune the strength of the interaction. We also need spatial coordinates $\vec{r}_j$ for all spins. For simplicity we arrange them on the unit circle

$$\vec{r}_j = \begin{pmatrix} \cos(2\pi j/N) \\ \sin(2\pi j/N) \\ 0 \end{pmatrix} \ . \tag{B2}$$

Figure 17 shows time evolutions for initial state $|\psi_B\rangle$ for two different parameters λ. As expected the spin expectation values decay the faster the larger the parameter λ is. But even for a small λ in Fig. 17(a) the spins do not synchronize at all. This can also be seen in the related video at [22].

$$\underset{\sim}{H} = \sum_{j=1}^{N} \sum_{k=j+1}^{N} \frac{\lambda}{r_{jk}^3} \left(\vec{\underset{\sim}{s}}_j \cdot \vec{\underset{\sim}{s}}_k - \frac{3(\vec{\underset{\sim}{s}}_j \cdot \vec{r}_{jk})(\vec{\underset{\sim}{s}}_k \cdot \vec{r}_{jk})}{r_{jk}^2} \right)$$
$$- h \sum_{j=1}^{N} \underset{\sim}{s}_j^z \ . \tag{B1}$$